Shear viscosity of degenerate electron matter

2008 J. Phys. A: Math. Theor. 41 205501

(http://iopscience.iop.org/1751-8121/41/20/205501)

IOP PUBLISHING JOURNAL OF PHYSICS A: MATHEMATICAL AND THEORETICAL

J. Phys. A: Math. Theor. **41** (2008) 205501 (13pp) doi:10.1088/1751-8113/41/20/205501

Shear viscosity of degenerate electron matter

P S Shternin

Ioffe Physical Technical Institute, Politekhnicheskaya 26, 194021 Saint-Petersburg, Russia

E-mail: pshternin@gmail.com

Received 17 December 2007, in final form 25 March 2008
Published 23 April 2008
Online at stacks.iop.org/JPhysA/41/205501

Abstract

We calculate the partial electron shear viscosity η_{ee} limited by electron–electron collisions in a strongly degenerate electron gas taking into account the Landau damping of transverse plasmons. The Landau damping strongly suppresses η_{ee} in the domain of ultrarelativistic degenerate electrons and modifies its temperature behavior. The efficiency of the electron shear viscosity in the cores of white dwarfs and envelopes of neutron stars is analyzed.

PACS numbers: 52.25.Fi, 97.20.Rp, 97.60.Jd

(Some figures in this article are in colour only in the electronic version)

1. Introduction

Transport properties of degenerate dense matter have been studied for a long time. They are especially important for simulating various processes in neutron stars, white dwarfs and degenerate cores of giant stars. All these objects contain a degenerate electron gas, and the electrons can contribute considerably to transport coefficients. Although the electron transport problem is very well elaborated and described in textbooks (e.g. [1]), some aspects have to be reconsidered.

The first studies of electron transport properties (thermal conductivity) of degenerate stellar matter were performed by Marshak [2], Mestel [3] and Lee [4] in the 1940s. Further work in the following two decades is described by Lampe [5] who made a considerable contribution to the calculation of the electron thermal conductivity. Later the subject was studied by many authors, particularly by Flowers and Itoh [6] and others [7–11]. However, all these authors have considered collisions of relativistic charged particles in the static limit. The importance of dynamical interactions for relativistic particles was pointed out by Heiselberg and Pethick [12] who analyzed transport properties of an ultrarelativistic quark plasma. The authors calculated transport coefficients of a degenerate ultrarelativistic plasma and showed that the results are qualitatively different from standard Fermi-liquid expressions because ultrarelativistic charged particles interact mainly through their currents. Such an interaction is

produced via the exchange of transverse plasmons (instead of the standard Coulomb charge–charge interaction of non-relativistic particles via the exchange of longitudinal plasmons). An inclusion of transverse plasmons increases the effective collision rates (decreases the kinetic coefficients).

Recently, we have reconsidered [13] the electron thermal conductivity of degenerate matter containing an electron gas of any degree of relativity. We have shown that a correct treatment of electron–electron collisions, including the exchange of transverse plasmons, increases the contribution of these collisions into the electron thermal conductivity.

In the present paper, we perform similar revision of the electron shear viscosity. Such a viscosity is important for studying hydrodynamical processes in neutron stars and white dwarfs, particularly the damping of oscillations of these objects. We will focus on the contribution from the electron–electron collisions. Our analysis will be similar to that in [12, 13]. Thus, we omit technical details.

The electron shear viscosity can be written as [1]

$$\eta_e = \frac{n_e v_e p_e}{5\nu_e}, \tag{1}$$

$$\nu_e = \nu_{ee} + \nu_{ei}, \tag{2}$$

where n_e is the electron number density, $p_e = \hbar(3\pi^2 n_e)^{1/3}$ and $v_e = p_e/m_e^*$ are, respectively, the electron Fermi-momentum and Fermi-velocity, m_e^* being the electron effective mass on the Fermi surface (it differs from bare electron mass due to relativistic effects). Furthermore, ν_e is the total electron effective collision frequency, a sum of the electron–ion collision frequency ν_{ei} and the electron–electron collision frequency ν_{ee}. Detailed calculations of ν_{ei} have been recently performed in [14], while ν_{ee} is the main subject of our study. After calculating η_{ee}, we briefly analyze the efficiency of η_e in the cores of white dwarfs and envelopes of neutron stars (particularly, for the damping of pulsations of pre-white dwarf and white dwarf stars).

2. Formalism

We consider an almost ideal and uniform strongly degenerate electron gas. The electrons can have any degree of relativity and collide among themselves and with plasma ions. To calculate the electron–electron collision frequency we use the standard variational approach with the simplest trial function [1]. The variational expression for the effective electron–electron collision frequency, that determines the shear viscosity, is

$$\nu_{ee} = \frac{15\pi^2\hbar^3}{8 v_e p_e^4 k_B T} \int \frac{\mathrm{d}\mathbf{p}_1\,\mathrm{d}\mathbf{p}_2\,\mathrm{d}\mathbf{p}_1'\,\mathrm{d}\mathbf{p}_2'}{(2\pi\hbar)^{12}} W(12|1'2') f_1 f_2 (1-f_1')(1-f_2') \times [p_{1x}v_{1y} + p_{2x}v_{2y} - p_{1x}'v_{1y}' - p_{2x}'v_{2y}']^2, \tag{3}$$

where T is the temperature and k_B is the Boltzmann constant. The integration is performed over all possible electron states involved in collisions $\mathbf{p}_1\mathbf{p}_2 \to \mathbf{p}_1'\mathbf{p}_2'$; $\mathbf{p}$ is an electron momentum, p_x being its component along the x-axis, v_y is the electron velocity component along the y-axis; primes indicate particle states after a collision; f is the Fermi-Dirac distribution function. Equation (3) includes the symmetry factor $1/2$ which excludes double counting of the same collision events of identical particles (electrons). Furthermore, $W(12|1'2')$ is the differential transition probability, summed over spin states of colliding particles,

$$W(12|1'2') = \frac{(2\pi\hbar)^4}{\hbar^2}\delta(\varepsilon_1' + \varepsilon_2' - \varepsilon_1 - \varepsilon_2)\delta(\mathbf{p}_1' + \mathbf{p}_2' - \mathbf{p}_1 - \mathbf{p}_2) \sum_{\text{spins}} |M_{fi}|^2, \tag{4}$$

where ε is the electron energy. The delta-functions reflect the momentum and energy conservation; $|M_{fi}|^2$ is the squared matrix element.

The matrix element M_{fi} for a collision of charged particles depends on the character of plasma screening of the electromagnetic interaction between these particles. For *ee* collisions (of identical particles), one has $M_{fi} = M_{fi}^{(1)} - M_{fi}^{(2)}$, where $M_{fi}^{(1)}$ and $M_{fi}^{(2)}$ correspond to two collision channels, $1 \to 1'; 2 \to 2'$ and $1 \to 2'; 2 \to 1'$, respectively, and

$$M_{fi}^{(1)} = \frac{4\pi e^2}{c^2}\left(\frac{J_{1'1}^{(0)} J_{2'2}^{(0)}}{q^2 + \Pi_l} - \frac{\mathbf{J}_{t1'1} \cdot \mathbf{J}_{t2'2}}{q^2 - \omega^2/c^2 + \Pi_t}\right). \tag{5}$$

In this case, $\hbar\mathbf{q} = \mathbf{p}_1' - \mathbf{p}_1$ and $\hbar\omega = \varepsilon_1' - \varepsilon_1$ are the momentum and energy transfers in a collision event, respectively; $J_{e'e}^{(\nu)} = \left(J_{e'e}^{(0)}, \mathbf{J}_{e'e}\right) = (2m_e^* c)^{-1}(\bar{u}_{e'}\gamma^\nu u_e)$ is the transition 4-current, $\mathbf{J}_{te'e}$ is the component of $\mathbf{J}_{e'e}$ transverse to $\mathbf{q}$; γ^ν is a Dirac matrix; u_e a normalized electron bispinor (with $\bar{u}_e u_e = 2m_e c^2$), and $\bar{u}_e$ is a Dirac conjugate. The expression for $M_{fi}^{(2)}$ is obtained from equation (5) by the interchange of indices $1' \leftrightarrow 2'$.

For collisions of strongly degenerate particles, calculations are simplified by placing all interacting particles on their Fermi surfaces (whenever possible). Characteristic values of q and ω in electron–electron collisions are determined by plasma screening, that is described by polarization functions Π_l and Π_t for the longitudinal (charge–charge) and transverse (current–current) interactions, respectively. The nature of plasma screening is discussed in [12, 13]. Let us summarize the main points. Usually, collisions of charged particles are studied in the so-called weak-screening approximation, in which momentum transfers are smaller than particle momenta. This approximation is justified by the long-range nature of electromagnetic interactions reflected in a specific q-dependence of the matrix element (5) (a well-pronounced peak at small q). As a result, only small values of q contribute to the integral (3), being determined by the character of plasma screening [12]. In the weak-screening approximation, it is sufficient to consider the polarization functions in the classical limit ($\hbar q \ll p_e$ and $\hbar\omega \ll v_e p_e$), in which they are given by [15]

$$\Pi_l = q_0^2 \chi_l(x), \qquad \Pi_t = (q_0 v_e/c)^2 \chi_t(x), \tag{6}$$

where $x = \omega/(q v_e)$,

$$\begin{aligned} \chi_l(x) &= 1 - \frac{x}{2}\ln\left(\frac{x+1}{x-1}\right), \\ \chi_t(x) &= \frac{x^2}{2} + \frac{x(1-x^2)}{4}\ln\left(\frac{x+1}{x-1}\right), \end{aligned} \tag{7}$$

$\hbar^2 q_0^2 = 4e^2 p_e^2/(\pi\hbar v_e)$, and q_0 is the Thomas–Fermi electron screening wavenumber. The longitudinal and transverse screenings are essentially different. The most striking difference occurs in a strongly degenerate plasma at temperatures T much below the electron plasma temperature $T_{pe} = \hbar\omega_{pe}/k_\mathrm{B}$ (that is determined by the electron plasma frequency $\omega_e = \sqrt{4\pi e^2 n_e/m_e^*}$). In this case, it is sufficient to consider the low-frequency limit of $\omega \to 0$ and $\omega/q \ll v_e$, in which

$$\chi_l = 1, \qquad \chi_t = \mathrm{i}\pi\omega/(4q v_e). \tag{8}$$

The longitudinal polarization function is real in this limit. It means, that the longitudinal electromagnetic interaction (via the exchange of longitudinal plasmons) results in the standard Debye-like screening with a characteristic momentum transfer $q_l \sim q_0$ (see equation (5)). For the transverse interaction (via the exchange of transverse plasmons), characteristic momentum transfer is different, $q_t \sim (\omega q_0^2/v_e)^{1/3}$. Moreover, the transverse polarization function is purely

imaginary. Accordingly, virtual transverse plasmons undergo collisionless absorption via the well-known Landau damping.

Comparing screening lengths in the low-energy limit, we see that $q_t \ll q_l$. Thus, transverse interactions occur on larger length scales than longitudinal ones and are, therefore, more frequent. In previous work on the electron shear viscosity, this difference between longitudinal and transverse interactions have been neglected and one set $\Pi_l = \Pi_t = q_0^2$. It is a good approximation in the non-relativistic case, because the ratio of the transverse to longitudinal parts of the matrix element in equation (5) contains a relativistic factor $\left(J_{te'e}/J^{(0)}_{e'e}\right)^2 \sim v_e^2/c^2$. Hence, transverse interactions of non-relativistic particles are inefficient. In contrast, the collisions of relativistic electrons via the exchange of transverse plasmons are more important than the collisions via the exchange of longitudinal plasmons (owing to larger screening length). This effect was analyzed by Heiselberg and Pethick [12] for a gas of ultrarelativistic quarks. Here, we consider the electron–electron collisions for any degree of electron relativity, in analogy with the study of [13] for the thermal conductivity.

Placing all colliding particles on their Fermi surfaces and performing possible analytical integrations with the aid of delta-functions, we finally obtain the following expressions for the electron–electron collision frequency and associated partial shear viscosity,

$$\nu_{ee} = \frac{12\alpha^2}{\pi\hbar} k_B T \frac{c^2}{v_e^2} I_\eta(u,\theta), \qquad \eta_{ee} = \frac{\pi\hbar n_e p_e v_e^3}{60\alpha^2 c^2 k_B T I_\eta(u,\theta)}. \tag{9}$$

Here, $\alpha = e^2/\hbar c$ is the fine structure constant, and

$$I_\eta(u,\theta) = \int_0^\infty \mathrm{d}w \frac{w\mathrm{e}^w}{(\mathrm{e}^w-1)^2} \int_0^1 \mathrm{d}x(1-x^2) \int_0^\pi \frac{\mathrm{d}\phi}{\pi}(1-\cos\phi) \times \left| \frac{1}{1+(x\theta/w)^2\chi_l(x)} - \frac{u^2(1-x^2)\cos\phi}{1-u^2x^2+u^2(x\theta/w)^2\chi_t(x)} \right|^2 \tag{10}$$

is a dimensionless function of two variables,

$$u \equiv v_e/c, \qquad \theta = \hbar v_e q_0/(k_B T) = \sqrt{3}T_{pe}/T; \tag{11}$$

ϕ is the angle between components of momenta $\mathbf{p}_{1t}$ and $\mathbf{p}_{2t}$ transverse to $\hbar\mathbf{q}$, and $w = \hbar\omega/(k_B T)$. Note, that in the small-momentum approximation, the interference term between $M^{(1)}_{fi}$ and $M^{(2)}_{fi}$ is small and both collision channels give equal contributions, resulting in $|M_{fi}|^2 \to 2|M^{(1)}_{fi}|^2$. Equations (9) and (10) generalize equations (47) and (48) from [12] to the case of arbitrary degree of relativity.

Integration over ϕ in equation (10) is straightforward and gives

$$I_\eta(u,\theta) = I_l(u,\theta) + I_t(u,\theta) + I_{tl}(u,\theta), \tag{12}$$

where I_l comes from the exchange of longitudinal plasmons, I_t from the exchange of transverse plasmons, and I_{tl} is the interference term.

Following [13], consider four regimes of collisions between degenerate electrons as indicated in table 1.

The regime I occurs in a non-relativistic ($v_e \ll c$) and rather warm (although degenerate) plasma ($T \gtrsim T_{pe}$). The analysis of (10) leads to the following asymptotic expressions valid in this regime:

$$I_l = \frac{2}{3}\left(\ln\frac{1}{\theta} + 1.919\right), \qquad I_t = \frac{8u^4}{35}\left(\ln\frac{1}{u\theta} + 3.413\right), \qquad I_{tl} = \frac{8u^2}{15}\left(\ln\frac{1}{\theta} + 2.512\right). \tag{13}$$

Table 1. Four regimes of shear viscosity η_{ee} of degenerate electrons.

Regime	Electron velocity	Temperature	Main contribution	T-dependence of η_{ee}
I	$v_e \ll c$	$T \gtrsim T_{pe}$	I_l	$[T \ln(T/T_{pe})]^{-1}$
II	$v_e \ll c$	$T \ll T_{pe}$	I_l	$1/T^2$
III	$v_e \approx c$	$T \gtrsim T_{pe}$	$I_l + I_t + I_{lt}$	$[T \ln(T/T_{pe})]^{-1}$
IV	$v_e \approx c$	$T \ll T_{pe}$	I_t	$1/T^{5/3}$

The leading contribution comes from I_l owing to a small relativistic factor u (as discussed above). The logarithmic terms and constant corrections in brackets are corresponding Coulomb logarithms (the corrections were calculated numerically). The leading-term result for η_{ee} in this regime is well known.

In the regime III, where the plasma is again warm ($\theta \gtrsim 1$), but the electron gas is ultrarelativistic ($u \approx 1$), I_l is the same as in the regime I (because I_l is independent of u). The asymptotic expressions for two other integrals have the same form as in the regime I but with different corrections,

$$I_t = \frac{1}{3}\left(\ln\frac{1}{\theta} + 2.742\right), \qquad I_{tl} = \frac{2}{3}\left(\ln\frac{1}{\theta} + 2.052\right). \tag{14}$$

Now all three terms give comparable contribution to I_η. The asymptote for I_η in the ultrarelativistic case coincides with that obtained by Heiselberg and Pethick [12]. It is different from the asymptote obtained by using an incorrect longitudinal screening in the transverse part of M_{fi}. However, the difference occurs only in the corrections to the dominant logarithmic terms.

The regimes II and IV are realized in a cold plasma ($\theta \ll 1$). In this case, we get

$$\begin{aligned} I_l &= \frac{\pi^3}{12\theta}, \\ I_t &= \xi\frac{u^{10/3}}{\theta^{2/3}}, \qquad \xi = \frac{\pi}{6}\left(\frac{4}{\pi}\right)^{1/3}\Gamma(8/3)\zeta(5/3) \approx 1.813, \\ I_{tl} &= \frac{\pi^3 u^2}{6\theta}, \end{aligned} \tag{15}$$

where $\zeta(z)$ is the Riemann zeta function and $\Gamma(z)$ is the gamma function. In the ultrarelativistic limit (the regime IV, $u = 1$), these expressions coincide with those obtained by Heiselberg and Pethick for an ultrarelativistic quark plasma [12].

The main contribution to I_η in the regime II comes from I_l due to a strong suppression of I_{tl} and I_t in the non-relativistic case. In the regime IV, which usually operates everywhere in the neutron star crust (excluding only a thin layer—a few meters—from the surface) and in the neutron star core, the situation is different. The leading term is then I_t, which corresponds to the exchange of transverse plasmons. It dominates because of smaller characteristic momentum transfers (larger electron mean-free paths) than those owing to the exchange of longitudinal plasmons. The temperature dependence of η_{ee} in the regime IV differs from the standard Fermi-liquid case (now $\eta_{ee} \propto T^{-5/3}$ instead of the standard dependence T^{-2}). The difference is smaller, than for the thermal conductivity κ_{ee} (κ_{ee} is remarkably independent of T in the regime IV while a standard Fermi-liquid requires $\kappa_{ee} \propto T^{-1}$). Therefore, the Landau damping affects the shear viscosity weaker than the thermal conductivity.

In addition to the above asymptotes, we have calculated I_l, I_t and I_{tl} on a dense grid of u and θ values covering transition regions between the regimes I–IV. We have further obtained the fit expressions which reproduce numerical results and asymptotic limits. The fit for I_l is

$$I_l = \left(0.379 + \frac{0.287}{1 + 0.165\theta + 0.0019\theta^2}\right) \ln\left(1 + \frac{6.81}{\theta}\right), \tag{16}$$

with the maximum fit error of 1.4% at $\theta = 1$ (let us recall, that I_l is independent of u).

The fit for I_t reads

$$I_t = \left[\frac{1.813}{C} + \frac{(C_2 - 1.813/C)(1 + 534\theta u - 764(\theta u)^2)}{1 + 705\theta u + 1630(\theta u)^2 + (3 + 3.4u^2)(\theta u)^3}\right] \times \ln\left[1 + \frac{C}{A(\theta u)^{1/3} + (\theta u)^{2/3}}\right], \tag{17}$$

where $C_1 = 0.7801 + 0.1337u^4$, $C_2 = 0.686 + 0.315u^4$, $A = 0.556 - 0.08u^2$, and $C = A\exp(C_1/C_2)$. The maximum error of 3.9% is at $\theta = 10^{-4}$, $u = 0.57$.

Finally, for I_{tl} we obtain

$$I_{tl} = \left[\frac{5.168}{D} + \frac{(D_2 - 5.168/D)(1 + p_1\theta - p_2\theta^2)}{1 + p_3\theta + p_4\theta^2 + p_5\theta^3}\right] \ln\left(1 + \frac{D}{\theta}\right), \tag{18}$$

where $p_1 = 15.2 - 16.5u^2$, $p_2 = 0.354 + 1.178u^2$, $p_3 = 13.5 - 13.68u^2$, $p_4 = 2.938 - 2.886u^2$, $p_5 = 0.003\,75 - 0.003\,73u^2$, $D_1 = 1.339 + 0.029u^4$, $D_2 = 0.533 + 0.133u^4$ and $D = \exp(D_1/D_2)$. The maximum error of 2.7% is at $\theta = 10^{-2}$, $u = 1$.

3. Discussion

Let us discuss the electron shear viscosity in a dense plasma. It is convenient to rewrite equation (1) as

$$\eta_e^{-1} = \eta_{ee}^{-1} + \eta_{ei}^{-1}, \qquad \eta_{ee} = \frac{n_e v_e p_e}{5\nu_{ee}}, \qquad \eta_{ei} = \frac{n_e v_e p_e}{5\nu_{ei}}, \tag{19}$$

where η_{ee} and η_{ei} are the partial viscosities governed by electron–electron and electron–ion collisions, respectively. We will discuss the effect of the Landau damping on η_{ee} and the contribution of η_{ee} in the total electron shear viscosity η_e. The partial viscosity η_{ei} will be calculated using the formalism of [14].

Figure 1 shows the temperature dependence of η_e in the helium and carbon plasma at $\rho = 10^6$ g cm^{-3} (where degenerate electrons become mildly relativistic). At higher ρ, the electrons are essentially relativistic and the effect of the Landau damping is most pronounced, see section 2. Densities $\rho \gtrsim 10^6$ g cm^{-3} are appropriate for degenerate cores of white dwarfs and red giants and for envelopes of neutron stars. We plot the partial shear viscosity η_{ee} (line 'ee') and the same viscosity, but retaining only collisions via the exchange of longitudinal plasmons (line 'ee-l'). These lines are the same for the helium and carbon plasmas. The relative contribution of collisions via the exchange of transverse plasmons in ν_{ee} increases when T falls below the electron plasma temperature T_{pe} ($\log_{10} T_{pe}[\mathrm{K}] \approx 8.32$, as indicated by the vertical dotted line in figure 1). The electron plasma temperature separates the high-temperature and low-temperature asymptotic regions (the regions III and IV for ultrarelativistic electrons, I and II for non-relativistic electrons, see table 1).

The dashed lines in figure 1 show η_{ei} and the solid lines marked 'tot' show the total electron viscosity η_e. One can see that the electron–electron collisions are more efficient at higher temperatures in a plasma containing lighter nuclei (more exactly, the nuclei of lower

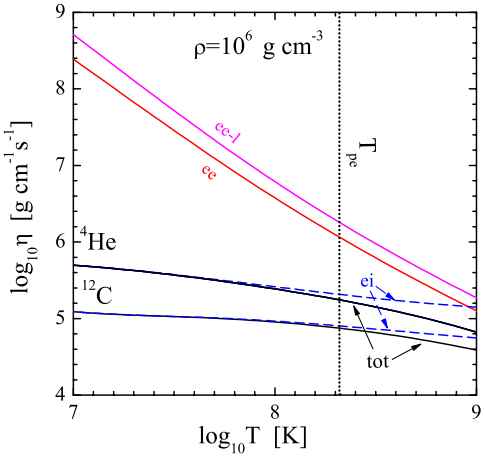

Figure 1. Temperature dependence of the electron shear viscosity at $\rho = 10^6$ g cm^{-3}. The line, marked 'ee', shows η_{ee}; the line 'ee-l' is the same, but only the contribution from the collisions via the exchange of longitudinal plasmons is retained. The dashed lines 'ei' and the solid lines 'tot' show η_{ei} and η_e, respectively, for helium and carbon plasmas. Vertical dotted line indicates the electron plasma temperature.

charge, such as He, whose interaction with electrons is especially weak). At the given $\rho = 10^6$ g cm^{-3}, the plasma screening type is not very important, and the collisions via the exchange of transverse and longitudinal plasmons give comparable contribution. With increasing ρ, the electron–electron collisions become also more important at temperatures below T_{pe}. However, at sufficiently high densities low-charge nuclei transform to those with higher charge (mainly owing to beta captures and nuclear fusion reactions). For these new nuclei with higher charge, the electron–electron collisions become less important.

At high densities in a neutron star envelope (crust) the composition of matter cannot be arbitrary and is determined by an evolution scenario for a given star. One usually considers the models of ground-state (cold catalyzed) crust or accreted crust (e.g., [16]). Figure 2 shows the density dependence of η_e, η_{ee} and η_{ei} throughout a neutron star crust (for $\rho > 10^9$ g cm^{-3}) at $T = 10^6$ K. We use a smooth composition model for the ground-state matter in the crust [16]. Let us recall that the crust extends to $\rho \sim 1.5 \times 10^{14}$ g cm^{-3}, while higher ρ correspond to a neutron star core composed of uniform neutron-rich nuclear matter. The vertical dotted line on the figure 2 shows the neutron drip point ($\rho_{nd} = 4.3 \times 10^{11}$ g cm^{-3}), which separates the outer crust (composed of electrons and nuclei) and the inner crust (where free neutrons appear in dense matter). The lines marked 'ee' and 'ee-l' again show η_{ee} calculated including and excluding the exchange of transverse plasmons, respectively. Correct values of η_{ee} are more than one order of magnitude lower than the values 'ee-l'. However, this suppression of η_{ee} by the Landau damping is insufficient for η_{ee} to dominate in η_e. The solid line marked 'no US' in figure 2 shows the total electron shear viscosity η_e in which η_{ei} is calculated under the same assumptions as in [14]. Most importantly, the calculations neglect the freezing of *Umklapp* processes of electron–ion (electron–phonon) scattering at low temperatures ($T \ll T_{pe}$) due to band-structure effects associated with the motion of the electrons in crystalline lattice. It turns out that η_{ei} is several orders of magnitude lower than η_{ee}, and, therefore, $\eta_e \approx \eta_{ei}$.

However, the freezing of *Umklapp* electron–phonon scattering processes is a delicate task which has not been studied in detail in the literature. If the freezing operates, it enhances

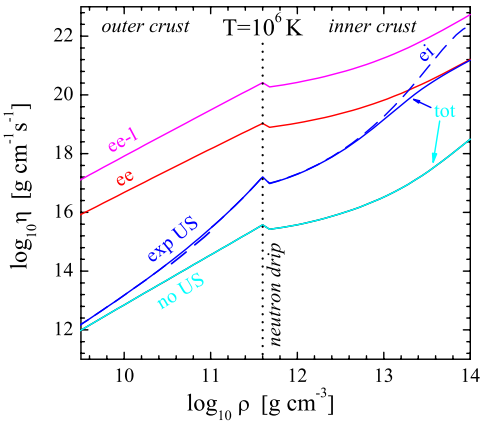

Figure 2. Density dependence of the electron shear viscosity in a neutron star crust composed of the ground-state matter at $T = 10^6$ K. The line, marked 'ee', shows η_{ee}; the line 'ee-l' is the same, but retaining the contribution from longitudinal plasmons alone. The dashed line 'ei' displays solid lines 'tot' give η_e. The lines 'no US' and 'exp US' are calculated neglecting the *Umklapp* suppression and assuming an exponential *Umklapp* suppression in electron–ion collisions, respectively. The vertical dotted line shows neutron drip point.

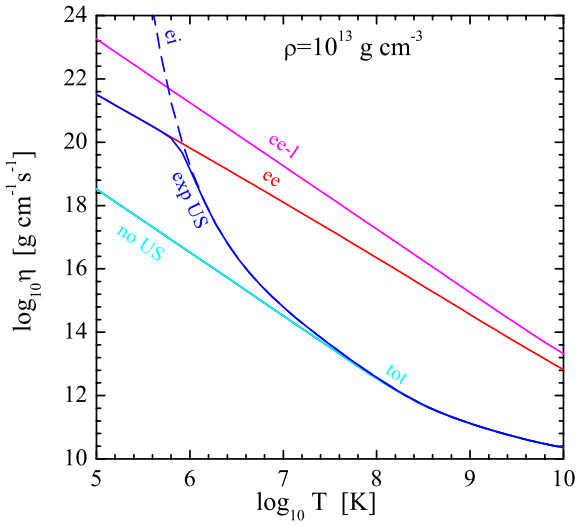

Figure 3. Temperature dependence of the electron shear viscosity in a neutron star crust composed of ground-state matter at $\rho = 10^{13}$ g cm^{-3}. Notations are the same as in figure 2.

η_{ei} and makes η_{ee} more important. To illustrate this effect, in figure 2 we present the η_e and η_{ei} curves, marked by 'exp US' and calculated assuming an exponential freezing of the electron–phonon scattering rate after T falls below some temperature T_u (that is approximately two orders of magnitude lower than ion plasma temperature). This illustrative model was used in [9] (and was described there in more detail). In this case the electron–electron collisions become significant at the bottom of a cold neutron star crust, at $\rho \gtrsim 10^{13}$ g cm^{-3}.

Figure 3 shows the temperature dependence of η_e, η_{ei} and η_{ee} at $\rho = 10^{13}$ g cm^{-3} (deep in the inner crust) under the same assumptions as in figure 2. If the freezing of *Umklapp*

processes is neglected, then even for very low temperatures $T \sim 10^5$–10^6 K (where η_{ee} is actually two orders of magnitude lower than η_{ee-l}), η_{ee} gives negligible contribution to η_e (figure 3; curves 'ee', 'ee-l' and 'tot', 'no US'). However, if one includes the freezing of *Umklapp* processes, then η_{ee} dominates at low T.

The suppression of *Umklapp* processes at $T \lesssim T_u$ can actually be non-exponential, but power-law [17], which will reduce the importance of the electron–electron collisions. This suppression is complicated and should be a subject of separate study. In addition, we have neglected the scattering of electrons by charged impurities. It can also be important at low temperatures (depending on charges and abundance of impurity ions, e.g., [18]) and it can further reduce the importance of η_{ee} (regardless the details of *Umklapp* freezing).

The contribution of electron–electron collisions to η_e is not so high as their contribution to the electron thermal conductivity κ_e [13]. This is because κ_{ee} strongly depends on the screening momenta than η_{ee}. As a result, the dynamical Landau damping introduces into κ_{ee} an additional factor proportional to T. In the asymptotic region IV, κ_{ee} becomes then temperature independent. In contrast, the Landau damping introduces into η_{ee} a much weaker factor $\propto T^{1/3}$.

When calculating the electron–electron collision rate we have neglected the ion contribution into the polarization functions Π_l and Π_t. It is a good approximation in the case of weak Coulomb coupling of ions $T \gtrsim Z^2e^2/(ak_B)$, when the ions constitute a nearly ideal Boltzmann gas ($a = (4\pi n_i/3)^{-1/3}$ being the ion-sphere radius, determined by the ion number density n_i). The calculation of the ion contribution to the plasma screening at lower temperatures $T \lesssim Z^2e^2/(ak_B)$ (where the ions form a Coulomb liquid or solid) is a complicated and unsolved problem. We have also neglected the effects of strong magnetic fields which can be available in neutron star envelopes and which can greatly modify the electron shear viscosity. These effects can be divided into two groups. First, they are the classical effects of electron magnetization owing to a fast electron rotation about magnetic field lines. Second, there are the effects of the Landau quantization of electron motion in a magnetic field (important usually for higher magnetic fields than the magnetization effects). The generalization of our solution to not too high magnetic fields, that do not affect the polarization functions, is straightforward. Stronger magnetic fields make the polarization tensor anisotropic, dependent on the magnetic field strength and direction. The effects of the ion polarization and strong magnetic fields on η_{ee} are beyond the scope of the present paper.

4. Shear viscosity in the cores of pulsating pre-white dwarf and white dwarf stars

Asteroseismology of white dwarfs is a rapidly developing field. More than 150 pulsating white dwarfs have already been observed (e.g., [19, 20] and references therein). The pulsation periods range from few minutes to few tens of minutes, and the relative pulsation amplitudes (pulsating fraction of star's luminosity) can be as high as a few percent. A comparison of the observed and theoretical pulsation frequencies allows one to identify pulsation modes, to accurately determine white dwarf masses and radii, and to explore their rotation, magnetic fields, internal structure and evolution.

All observed pulsation modes are interpreted as non-radial gravity modes (g-modes, produced owing to buoyancy forces) of multi-polarity $\ell = 1, 2$ with $k = 1, \ldots, 50$ radial nodes. They are excited in the envelopes of young warm pre-white dwarfs and white dwarfs presumably by the instability that is mainly associated with the partial ionization of the plasma.

Pulsating pre-white dwarfs (called PG 1159, or GW Vir stars) have the effective surface temperatures $T_{\rm eff}$ from $\simeq$ 170 000 K to 75 000 K. They are hot, young stars (of age $\lesssim 10^5$ yr), still contracting slowly in the course of cooling because of a not too strong electron

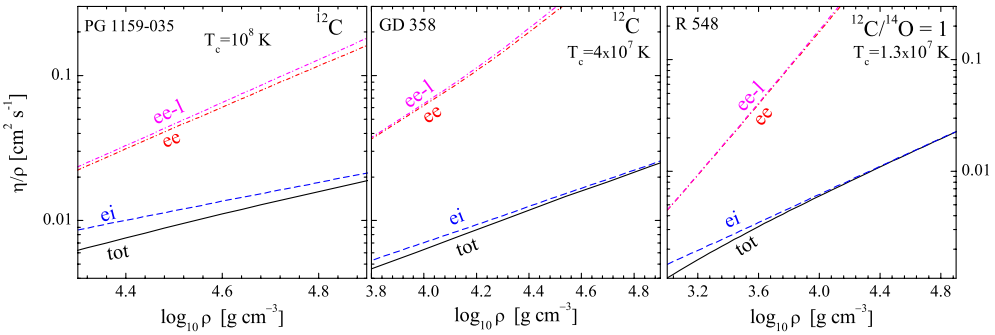

Figure 4. Kinematic shear viscosity η/ρ in the core of the pre-white dwarf PG 1159–035 (left), the DBV white dwarf GD 358 (middle) and the DBA white dwarf R 548 (right). The curves 'tot' show the total viscosity; the curves 'ei' and 'ee' are the contributions of electron–ion and electron–electron collisions, respectively. Lines 'ee-l' refer to electron–electron collisions retaining the exchange of longitudinal plasmons alone. The vertical scale on the right panel is different (shown on the right axis).

degeneracy in their cores. Their pulsations are thought to be driven by the partial ionization of C and O in the respective layers (which requires high $T_{\rm eff}$). In pulsating white dwarfs with helium atmospheres (DBV, or V777 Her stars), $T_{\rm eff}$ ranges from $\simeq$29 000 K to 22 000 K; these pulsations are excited in the He partial ionization zone. Pulsating white dwarfs with hydrogen atmospheres (DAV, or ZZ Ceti stars) have $T_{\rm eff}$ from $\simeq$12 500 K to 10 500 K. Their pulsations are most probably excited by convection in the outer layer with the partial ionization of hydrogen. Also, there exists a population of pulsating white dwarfs which belong to cataclysmic variables (accreting binaries). These white dwarfs have different composition of surface layers (contaminated by accretion from a companion star). As a result, they have different partial ionization zones, and their pulsations can be excited in a wide range of $T_{\rm eff}$ (from 10 000 K to 20 000 K and higher).

Let us analyze the shear viscosity in the cores of pulsating white dwarfs. This viscosity participates in the damping of those pulsations which penetrate into the core. In a steadily pulsating star (whose pulsations are generated by a driving force) the viscosity can limit the pulsation amplitude.

For illustration, in figure 4 we plot the density dependence of the kinematic shear viscosity η/ρ in the cores of three pulsating stars (three panels)—one pre-white dwarf and two white dwarfs. A solid curve marked 'tot' on each panel presents the total electron viscosity η/ρ, while dashed and dash-dotted curves 'ei' and 'ee' are the partial contributions of electron–ion and electron–electron collisions, respectively; a dash-dotted line 'ee-l' is the electron–electron contribution owing to the exchange of longitudinal plasmons alone.

The left panel of figure 4 corresponds to the conditions in the core of the extremely hot pulsating pre-white dwarf PG 1159–035. Its pulsation spectrum is rich; one has identified $\approx$200 pulsation modes [21]. An analysis of astroseismological and spectral observations gives, among other things, the effective surface temperature $T_{\rm eff} \approx 140\,000$ K, and the star's mass $\approx 0.6\,M_\odot$ [21]. According to the theory [22], the internal temperature of this star is mainly determined by the neutrino emission; it is nearly constant over the core, being close to the central temperature $T_c \approx 10^8$ K. Thus, we have plotted the shear viscosity for the isothermal degenerate core assuming pure carbon composition. At the lowest density on the figure, the electron degeneracy becomes mild (while our results are limited by a strong degeneracy). One can see that the electron–electron contribution to the electron shear viscosity is important only

in the outer core, at $\rho \lesssim 10^5$ g cm^{-3}. The contribution of the electron–electron collisions due to the exchange of transverse phonons is small, but noticeable. It reduces the total electron viscosity η_e, maxiumum by a factor of 1.5, and the reduction decreases with growing ρ.

The middle panel of figure 4 is appropriate for the conditions in the core of the pulsating DBV white dwarf GD 358. It was the first DBV pulsating dwarf observed, with at least ten well-identified pulsation modes [23] ($\ell = 1, k \lesssim 20$). Observations of GD 358 yield its mass $\approx 0.6\, M_\odot$ and the effective surface temperature $T_{\rm eff} \approx 24\,000$ K. These parameters and evolutionary models, reviewed in [24], imply the central temperature $T_c \approx 4 \times 10^7$ K and the central density $\rho_c \approx 2 \times 10^6$ g cm^{-3}. We have evaluated the shear viscosity (figure 4) using an appropriate theoretical temperature profile in the white dwarf core from [24]. For illustration, we have selected the pure carbon composition of the degenerate core. One can see, that the electron–electron contribution $\eta_{\rm ee}$ to the total electron shear viscosity η_e is now less important, about 10–20%. The boundary of the degenerate core shifts now to lower densities (to $\rho \sim 3 \times 10^3$ g cm^{-3}); the contribution of the electron–electron collisions via the exchange of transverse plasmons is lower.

Finally, the right panel of figure 4 shows the shear viscosity for the conditions in the core of the pulsating DAV white dwarf R 548. The observational data imply $T_{\rm eff} \approx 12\,000$ K, and, again, the white dwarf mass $\approx 0.6\, M_\odot$. The theory [24] predicts a nearly isothermal degenerate core with the temperature $T \approx T_c \approx 1.3 \times 10^7$ K. We have calculated the shear viscosity assuming the C–O core with equal mass fractions of C and O. The shear viscosity η_{ei}, limited by electron–ion collisions in a C–O mixture, has been determined using the linear mixing rule [16]. The contribution of collisions via the exchange of transverse plasmons is now noticeable only at $\rho \lesssim 4 \times 10^3$ g cm^{-3}.

Our three examples in figure 4 cover a representative range of pulsating pre-white dwarf and white dwarf models. In all the cases the kinematic electron shear viscosity η/ρ is of the same order of magnitude, with characteristic values of $\eta/\rho \sim 10^{-3} - 10^{-2}$ cm^2 s^{-1}. If the damping of g-modes were solely determined by shear viscosity in the stellar core, a typical damping time could have been estimated as $\tau_{\rm shear} \sim \lambda^2 \rho/\eta$, where λ is a length scale of pulsation modes. Characteristic length scales are $\lambda \sim R/k \sim (0.1 - 0.01)R$, where $R \sim 10\,000$ km is the white dwarf radius and k is the number of radial oscillation nodes. This gives $\tau_{\rm shear} \sim 10^8$–$10^{11}$ yr, indicating that the shear viscosity in the cores of pulsating white dwarfs is rather inefficient in damping observed pulsations. It would be equally inefficient to damp other possible large-scale hydrodynamic motions in white dwarf cores (for instance, differential rotation).

The shear viscosity in white dwarf cores should have much stronger effect on small-scale motions. For instance, these could be small-scale (high-k or high-ℓ) pulsations, or ordinary pulsations in stratified cores, containing sharp boundaries between different layers (e.g., separating phases of different elements or phases of solidified and liquid matter). Viscous dissipation in boundary layers can be strong.

Similar conclusions can be made on the efficiency of the electron shear viscosity in the envelope (crust) of neutron stars (where one typically has $\eta_e/\rho \sim 0.01$–100 cm^2 s^{-1} for the range of the internal crust temperature from $\sim 10^9$ K to 10^7 K [14]). The viscosity η_e there is not too high and cannot be a strong regulator of large-scale motions (pulsations). Nevertheless, characteristic length scales in neutron stars are naturally much shorter than in white dwarfs (because neutron stars are smaller, and their crust thickness is $\lesssim 1$ km). This increases the efficiency of the shear viscosity (decreases viscous damping times) in neutron star envelopes (as compared to white dwarf cores). Moreover, a neutron star crust has a well-defined heterogeneous (multi-layer) structure [16], where viscous boundary layers can occur and viscous dissipation can be strong. Such effects are currently almost unexplored.

5. Conclusion

We have calculated the partial electron shear viscosity η_{ee} owing to collisions between degenerate electrons in a dense degenerate plasma taking into account the Landau damping of transverse plasmons. Our main conclusions are:

(1) The Landau damping reduces η_{ee} for all temperature and density regions I–IV (table 1).
(2) The strongest reduction occurs in the region IV of cold ($T \lesssim T_{pe}$) relativistic ($\rho \gg 10^6$ g cm^{-3}) electron plasma. In this region, the Landau damping lowers the viscosity η_{ee} by several orders of magnitude and modifies its temperature dependence (which becomes $\eta_{ee} \propto T^{-5/3}$ instead of the traditional dependence $\eta_{ee} \propto T^{-2}$).
(3) The viscosity η_{ee} gives a noticeable contribution to the total electron viscosity η_e in a plasma of light ions at $T \gtrsim T_{pe}$.
(4) The viscosity η_{ee} can also give a significant contribution to η_e in a deep crust ($\rho \gtrsim 10^{13}$ g cm^{-3}) of a cold neutron star ($T \lesssim 10^7$ K) provided crystalline lattice of atomic nuclei is rather pure and the freezing of *Umklapp* processes at low T is sufficiently strong. Both factors, the impurity of crystals and the character of *Umklapp* freezing, are currently uncertain and require special study.

We have approximated our results by simple analytic expressions which are valid in the wide range of densities and temperatures appropriate to degenerate cores of white dwarfs and red giants and to the envelopes of neutron stars. The analytic approximations can be easily incorporated into computer codes to simulate hydrodynamical processes in these stars. We have briefly analyzed (section 4) the efficiency of viscous damping in the cores of white dwarfs and envelopes of neutron stars.

The contribution of collisions of degenerate electrons via the Landau damping during the exchange of transverse plasmons has been neglected in all previous considerations of the electron shear viscosity. In the context of transport properties of dense quark plasma it was studied by Heiselberg and Pethick [12]. We have recently reconsidered the effect of the Landau damping on the electron thermal conductivity in neutron star crust and core [13, 25]. The same effect on the shear viscosity in the neutron star core (taking into account possible superfluidity of nucleons) will be studied in a similar way and published elsewhere.

Acknowledgments

I am grateful to AI Chugunov for sharing with me unpublished results and for noting the mislead in the preliminary version of the paper. This work was partially supported by the Dynasty Foundation, the Russian Foundation for Basic Research (grants 08-02-00837, 05-02-22003), and by the Federal Agency for Science and Innovations (grant NSh 2600.2008.2).

References

[1] Ziman J M 1960 *Electrons and Phonons* (Oxford: Oxford University Press) (chapter 9)
[2] Marshak R E 1941 *Ann. New York Acad. Sci.* **41** 49
[3] Mestel L 1950 *Proc. Camb. Phil. Soc.* **46** 331
[4] Lee T D 1950 *Astrophys. J.* **111** 625
[5] Lampe M 1968 *Phys. Rev.* **170** 306
[6] Flowers E and Itoh N 1976 *Astrophys. J.* **206** 218
[7] Timmes F X 1992 *Astrophys. J.* **390** 107
[8] Urpin V A and Yakovlev D G 1980 *Sov. Astron.* **24** 126
[9] Gnedin O Y, Yakovlev D G and Potekhin A Y 2001 *Mon. Not. R. Astron Soc.* **324** 725

[10] Yakovlev D G and Shalybkov D A 1991 *Astrophys. Space Sci.* **176** 171
Yakovlev D G and Shalybkov D A 1991 *Astroph. Space Sci.* **176** 191
[11] Gnedin O Y and Yakovlev D G 1995 *Nucl. Phys.* A **582** 697
[12] Heiselberg H and Pethick C J 1993 *Phys. Rev.* D **48** 2916
[13] Shternin P S and Yakovlev D G 2006 *Phys. Rev.* D **74** 043004
[14] Chugunov A I and Yakovlev D G 2005 *Astron. Rep.* **49** 724
[15] Alexandrov A F, Bogdankevich L S and Rukhadze A A 1984 *Principles of Plasma Electrodynamics* (Berlin: Springer) (chapter 4)
[16] Haensel P, Potekhin A Y and Yakovlev D G 2007 *Neutron Stars: 1. Equation of State and Structure* (New York: Springer) (chapter 3)
[17] Chugunov A I 2008 private communication
[18] Potekhin A Y, Baiko D A, Haensel P and Yakovlev D G 1999 *Astron. Astrophys.* **346** 345
[19] Kepler S O 2007 *Comm. Asteroseismol.* **150** 221
[20] Winget D E 1998 *J. Phys. Condens. Matter* **10** 11247
[21] Costa J E S *et al* 2008 The pulsation modes of the pre-white dwarf PG 1159–035 *Astron. Astrophys.* **477** 627
[22] O'Brien M S and Kawaler S D 2000 *Astrophys. J.* **539** 372
[23] Bradley P A and Winget D E 1994 *Astrophys. J.* **430** 850
[24] Tassoul M, Fontaine G and Winget D E 1990 *Astrophys. J. (Suppl.)* **72** 335
[25] Shternin P S and Yakovlev D G 2007 *Phys. Rev.* D **75** 103004